

Simulations of the thermo-acoustic lens effect during focused ultrasound surgery

Ibrahim M. Hallaj^{a)}

Radiology Department, Brigham & Women's Hospital, Harvard Medical School, 221 Longwood Avenue, Boston, Massachusetts 02115

Robin O. Cleveland

Department of Aerospace and Mechanical Engineering, Boston University, 110 Cummington Street, Boston, Massachusetts 02215

Kullervo Hynynen

Radiology Department, Brigham & Women's Hospital, Harvard Medical School, 221 Longwood Avenue, Boston, Massachusetts 02115

(Received 3 March 2000; revised 6 July 2000; accepted 5 February 2001)

Laboratory measurements of soft tissue properties show a dependence of background propagation properties on temperature. For typical focused ultrasound surgery (FUS) applications, only the slow variations in tissue background parameters need to be accounted for when computing the outcome of a FUS sonication. The cumulative effect of slowly varying sound speed has been referred to in the literature as a thermal lens, or a thermo-acoustic lens because of its beam-distorting properties. An algorithm to solve the coupled acoustic-thermal problem is described, and numerical results are presented to illustrate the effects of dynamic sound-speed profiles in layered tissues undergoing FUS. The results of simulations in liver with and without a fat layer indicate that the thermal-acoustic interaction results in more complex dynamics in FUS than a simple model will predict. Both the size and the position of the lesions predicted from the simulations are affected by the thermo-acoustic lens effect. However, the overall effect from short sonications at high power from sharply focused single element sources (F -no. from 0.8 to 1.3) around 1 MHz similar to those used in clinical setups is found to be small. © 2001 Acoustical Society of America. [DOI: 10.1121/1.1360239]

PACS numbers: 43.80.Gx, 43.80.Sh, 43.25.Cb, 43.25.Ed [FD]

I. INTRODUCTION

Minimally invasive tumor coagulation using focused ultrasound devices holds great promise in treating patients without the need for traditional surgical procedures.¹⁻³ The heating of soft tissues for therapeutic purposes has been demonstrated experimentally⁴⁻⁷ and explained theoretically.^{6,8-10}

Modeling of FUS systems is important for proper selection of device operating parameters and geometries. Numerical models provide a means of exploring thermal therapy treatment planning as well as system design. Models have been presented describing the behavior of focused ultrasonic beams in biological tissue^{11,12} and the thermal effect of such beams.¹³⁻¹⁶ Experiments in phantoms and *in vivo*¹⁷⁻²⁰ have been conducted to verify these models. Soft tissue is commonly modeled as a lossy fluid media,^{15,8} and the main effects of ultrasound on soft tissues can be described assuming compressional waves in fluids.

Some interesting phenomena have been observed in biomedical acoustics which suggest revisiting the traditional models when dealing with time-varying tissues. One such phenomenon is the thermo-acoustic lensing which occurs in

heated tissue, where a gradual movement in the position of the focus and a change in the local index of refraction occurs. This phenomenon may be partially explained as resulting from the temperature-dependence of the sound speed in tissue.²¹⁻²³ The acoustic intensity field generated from focused sources results in spatially inhomogeneous temperature fields in otherwise homogeneous tissue samples. Modeling such behavior requires using inhomogeneous equations to describe the acoustic and the thermal problems, and a mechanism for feedback between them.

In this paper an acoustic model incorporating inhomogeneity, absorption, and nonlinearity is used in conjunction with the bioheat transfer equation (BHTE) to predict acoustic and temperature fields in layered tissues with temperature-dependent sound speeds. The present paper deals with the coupling of the acoustic and the thermal problems via the sound speed of layered tissue in thermal therapy. While experimental data for tissue parameters as a function of temperature and thermal dose remain scarce, the data published for sound speed in fat and liver as a function of temperature are used to guide the time-domain simulations presented.

II. MODEL DESCRIPTION

A. The acoustic model

A second-order wave equation for finite-amplitude propagation in a thermo-viscous fluid is used as a model for

^{a)} Author to whom correspondence should be addressed, currently with Wolf, Greenfield & Sacks, P.C., 600 Atlantic Ave., Boston, MA 02210; electronic mail: ibrahim@alumni.washington.edu

TABLE I. Base values of acoustic parameters used in the study (37 °C).

Material	ρ (kg m ⁻³)	c_0 (m s ⁻¹)	α_0 (Np m ⁻¹ MHz ⁻¹)	β_0
Water	1000	1500	2.88×10^{-4}	3.5
Liver	1050	1596	4.5	6.0
Fat	910	1430	9.0	10.5

ultrasound propagation in this study. The equation is a generalized Westervelt equation, described in Hamilton and Morfey,²⁴

$$\nabla^2 p - \frac{1}{c_0^2} \frac{\partial^2 p}{\partial t^2} - \frac{1}{\rho} \nabla p \cdot \nabla \rho + \frac{\delta}{\rho c_0^4} \frac{\partial^3 p}{\partial t^3} + \frac{\beta}{\rho c_0^4} \frac{\partial^2 p^2}{\partial t^2} = 0. \quad (1)$$

The acoustic pressure p was calculated from the wave equation, given the material properties of the medium. The background density and sound speed of the medium are ρ and c_0 , respectively. The nonlinearity coefficient, β , is related to the nonlinearity parameter, B/A , by $\beta = 1 + (B/2A)$,²⁵ and the acoustic diffusivity, δ , accounts for both thermal and viscous losses in the fluid, and is related to the absorption coefficient by $\delta = 2\alpha c_0^3 / \omega^2$, where α is the acoustic absorption coefficient and ω is the angular frequency. It is assumed that the time rates of change of the background parameters in Eq. (1) are slow enough so that the extra terms in the wave equation for time-varying media are negligible. This slow time-varying background assumption has been shown to be reasonable for typical FUS applications.²⁶

For this study, the numerical solution of the wave equation in polar cylindrical coordinates is accomplished using the finite-difference time-domain (FDTD) method as described in Ref. 27. The partial derivatives in Eq. (1) are discretized to second-order accuracy in time and fourth-order accuracy in space with absorbing boundary conditions at the computational domain's edges. Table I gives the baseline values used for the acoustic parameters in Eq. (1). The data used in this study for the tissue parameters can be found in the literature, for example, in Goss *et al.*²⁸

B. The thermal model

The temperature increase in soft tissues can be modeled by a diffusion type equation. The Pennes bioheat transfer equation (BHTE)¹³ is used to describe the thermal effects of ultrasound in tissue:

$$\frac{\partial T}{\partial t} = \frac{k_t}{\rho C_t} \nabla^2 T - \frac{W_b C_b}{\rho C_t} (T - T_a) + \frac{Q}{\rho C_t}, \quad (2)$$

where T is the temperature in the tissue, k_t is the thermal conductivity of the tissue, C_t and C_b are the heat capacities of tissue and blood, respectively, W_b is the perfusion, T_a is the ambient (arterial) temperature (37 °C), and Q is the heat deposition source term due to the acoustic field. The heat source term was calculated as described by Pierce,²⁹

$$Q = \frac{\delta}{\rho_0 c_0^4} \left\langle \left(\frac{\partial p}{\partial t} \right)^2 \right\rangle. \quad (3)$$

Q was time-averaged over an acoustic period by numerical integration for use in the bioheat equation. Table II gives the

TABLE II. Base values of thermal parameters used in the study (37 °C).

Material	k (W m ⁻¹ K ⁻¹)	C (J kg ⁻¹ K ⁻¹)	W (kg m ⁻³ s ⁻¹)	T_a (°C)
Water	0.60	4180	0	37
Liver	0.50	3700	0.5	37
Fat	0.50	3700	0.5	37

reference values used for the parameters in Eq. (2).

The BHTE was solved in cylindrical coordinates using the FDTD method to the same accuracy as the wave equation. Constant flux boundary conditions were assumed for the edges of the computational domain to simulate an extended thermal region beyond the computational boundaries of the simulations, as constant temperature boundary conditions can create artifacts at the edges of the domain.

The temperature field was used to calculate thermal dose according to the formula

$$t_{43} = \int_{t=t_0}^{t=t_{\text{final}}} R^{(43-T(t))} dt. \quad (4)$$

after Sapareto and Dewey.³⁰ Here t_{43} is the thermal dose equivalent time at 43 °C, and t_0 and t_{final} are the starting and ending times of the sonication, and R is 0.5 if $T \geq 43$ °C, and 0.25 if $T < 43$ °C. Models commonly consider 240 min at 43 °C the threshold for lesion formation in soft tissue. This assumption has been tested against measured lesion sizes and found to be reasonable in soft tissues.⁶

C. Tissue response model

The data for sound speed as a function of temperature were compiled from measurements by Bamber and Hill.³¹ These data were adapted for the present study by using one data point per 5 °C according to the trends apparent from the published values. The results are shown in Fig. 1. The polynomials used in this study to fit the sound speeds in fat and liver to the experimental data are

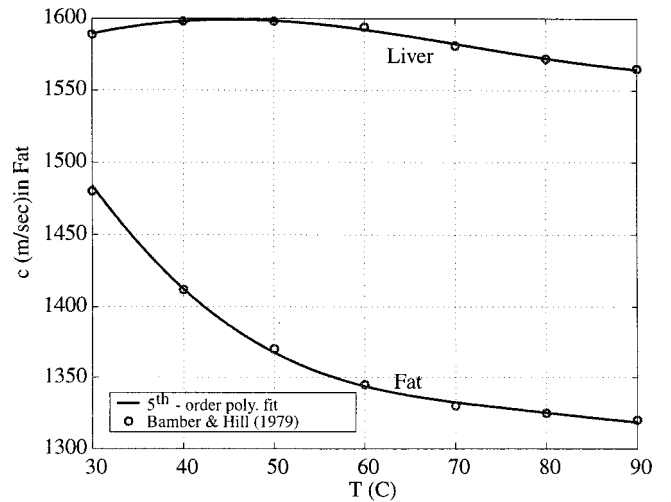


FIG. 1. Temperature dependence of sound speed in soft tissue taken from published laboratory measurements (symbols) and the corresponding polynomial fits to the data (solid).

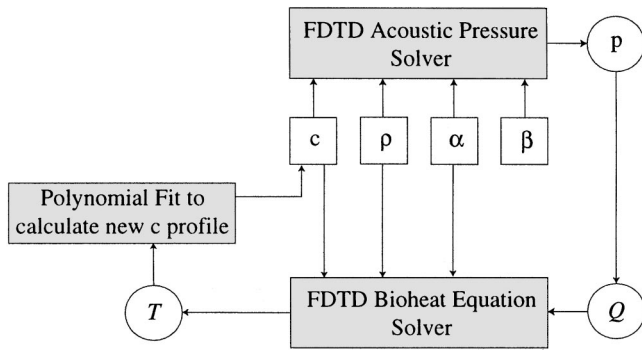


FIG. 2. Flowchart showing the iterative method for coupling the pressure and temperature calculations in the time-varying tissue simulations.

$$c_{\text{fat}}(T) = 1746 - 3.931T - 0.4128T^2 + 1.137 \times 10^{-2}T^3 - 1.101 \times 10^{-4}T^4 + 3.731 \times 10^{-7}T^5 \text{ m/s}, \quad (5)$$

$$c_{\text{liver}}(T) = 1529 + 1.686T + 6.113 \times 10^{-2}T^2 - 2.297 \times 10^{-3}T^3 + 2.266 \times 10^{-5}T^4 - 7.179 \times 10^{-8}T^5 \text{ m/s}. \quad (6)$$

The polynomial expressions are only valid inside the interpolation region, 30 °C to 90 °C.

These data imply that during the course of a single focused ultrasound treatment of finite duration the sound speed will change, and this change is considered in subsequent calculations of the acoustic and thermal fields.

D. Acousto-thermal coupling

The flowchart in Fig. 2 shows how the acoustic and the thermal solvers were coupled for the present computations via the heating term $Q(\mathbf{x}, t)$ in Eq. (3). Periodically the thermal solver was made to calculate and output the updated background sound speed of the tissue to data files. The sound speeds were calculated using the polynomial fits described above at each point in space on the computational domain. The updated $c(\mathbf{x}, t)$ profile was then used as an input to the acoustic solver to calculate a new pressure field in an iterative fashion. Thus the pressure field, which drives the heating, was in turn affected by the temperature field, and so forth. The tissue parameters and CW pressure field were updated for the simulations presented here every 2 s unless otherwise noted. This update period was determined to be sufficient for the FUS problems based on a convergence test in which the periodicity of updating was varied.

III. DESCRIPTION OF THE SIMULATIONS

The basic layout for the simulations is shown in Fig. 3 and involves a single element spherical section bowl transducer in water with axis of symmetry, z . The bowl has a radius of curvature which varied between 3.2 and 5.2 cm, an aperture diameter of 4 cm, and frequency of 1.0 MHz unless otherwise noted. F -numbers between 0.8 and 1.3 were used in the simulations to mimic the focused source conditions used in FUS devices. A simulation was also carried out for a 1.5 MHz source with an F -number of 1.0 for comparison. Another simulation spanning 60 s was done to assess the

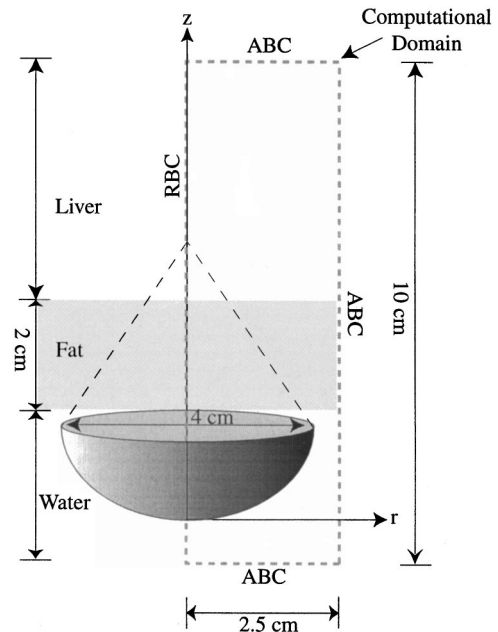


FIG. 3. Configuration used for the simulations showing the relative locations of the focused source and the water, fat, and liver layers. ABC denotes absorbing boundary conditions, and RBC denotes reflected symmetry boundary conditions. Not to scale.

effect of longer sonications in which prefocal heating can be more important than the brief high-power sonications. All sonications were adjusted for source pressure so that the final peak temperature at the focus was 80 ± 1 °C. This was based on the typical desired heating pattern for individual FUS sonications in clinical situations, chosen to avoid tissue boiling.

The calculations were carried out on a uniform grid with spatial discretization of 0.1 mm along both the radial and the axial directions. The computational domain spans a 10 cm (axial) by 2.5 cm (radial) area. However, due to the axial symmetry of the problem, the results are correct for a rotation of this 2-D space about the axis. The acoustic simulations used a time step of 10 ns, while the thermal simulations used a time step of 0.1 s. The reason for the disparity being that the acoustic FDTD code needed to resolve much shorter time scales associated with an acoustic period while the thermal FDTD code was used to compute heat transfer phenomena at much longer time scales.

The acoustic pressure, intensity, temperature, and sound-speed scalar fields were tracked and stored at 2 s intervals for a total run time of 10 s in the following simulations unless otherwise noted. The acoustic code was run until a steady-state CW field was obtained on the computational domain (about 100 μ s). This technique of using absorbing boundary conditions to obtain CW results from transient codes provided good convergence and has been shown to be successful for acoustic problems.³² The BHE code was then run using the most up-to-date values calculated for sound speed of 2 s, then the acoustic code was run again until steady state was reached, and so on. The results provide a sequence of pressure and temperature fields, as well as the evolving sound-speed profiles of the inhomogeneous tissues.

The source was simulated to be in water at 37 °C, and

TABLE III. Simulation parameters, including source powers, source pressures, and focal intensities which were required to achieve 80 °C peak temperature at the end of each CW sonication.

f (Mhz)	F -no.	Duration (s)	cm Fat	Power (W)	p_{source} (MPa)	I_{focus} (W m^{-2})
1.0	0.8	10	0	66.1	0.38	3183
1.0	0.8	10	2	78.2	0.41	3764
1.0	1.0	10	0	82.1	0.43	2650
1.0	1.0	10	2	98.1	0.47	3166
1.5	1.0	10	2	65.2	0.38	4749
1.0	1.0	60	2	60.5	0.37	1951
1.0	1.3	10	2	128.1	0.55	2565
1.0	1.3	10	3.5	140.1	0.57	2565

projecting a beam into soft (liver) tissue either directly adjacent to the water or separated from the water by a fat layer. Each of the layers was taken to be initially homogeneous and at 37 °C. Upon insonation by the acoustic field the tissue layers' sound speeds were assumed to evolve in space and time according to Eqs. (5) and (6). The water temperature and properties were kept constant, assuming that a regulated supply of cooling water was available. Table III shows the values of the pressures, powers, and intensities used for the simulations. For each case, the source pressure was arrived at by an iterative process using interpolation such that an 80 °C peak temperature was achieved at the focus at the end of the sonication, as stated earlier. The parameters and dimensions in Table III were considered representative of possible clinical therapeutic ultrasound treatment systems and tissue samples.

Separate simulations were conducted which did not take into account the acousto-thermal lensing for comparison. In these simulations the water and tissue layers were sonicated for the same duration with the same sources and powers, but the sound speeds were never altered from their baseline values during the heating.

IV. RESULTS

A. Short (10 s) CW sonications at 1.0 MHz, F no.=0.8, 1.0

Simulation results are presented as axial profiles of peak pressure, temperature, and sound speed evolving over the 10 s sonications. The profiles in Figs. 4–7 are plotted at 2 s intervals to illustrate the dynamics of the problem for the 1 MHz, F no.=0.8 and F no.=1.0 cases with and without a 2 cm thick fat layer.

Several main observations can be made from the peak pressure slices: First, the location of the peak pressure (the acoustic focus) drifts slightly in time toward the source. The position of the peak pressure does not drift by more than 2 mm for any of the 1 MHz, 10 s runs, and is only a fraction of a millimeter for the cases with no fat layer. The drift is due to the refraction of the rays as they propagate through the thermo-acoustic lens. The rate of drift appears to decrease over the course of a simulation because the temperature rise levels off during a sonication as conduction and perfusion act to limit the temperature rise. Standing waves were seen in the water and in the fat layer. No standing waves were seen in the liver tissue, as it was assumed to be unbounded using the absorbing boundary conditions. From the temperature

data we can see the drift of the hot spot toward the transducer as time progresses, mirroring the change in the acoustic pressure field.

The sound-speed variation was most remarkable in the fat layer, where the temperature dependence was most pronounced. The sound speed in fat underwent a change from its baseline value of 1430 m/s down to 1330 m/s near the focus after 10 s of heating. The main observations from the sound-speed profiles from the simulations are the fact that generally the sound speeds in tissue and liver (above 45 °C) drop near the focus as the temperature increases. A slight increase was seen at the periphery of the focal zone as the liver was heated only slightly, and was on the $c(T)$ region of the curve in which sound speed climbs to a local maxima near 45 °C. Also noted was the way in which the sound speed in the fat

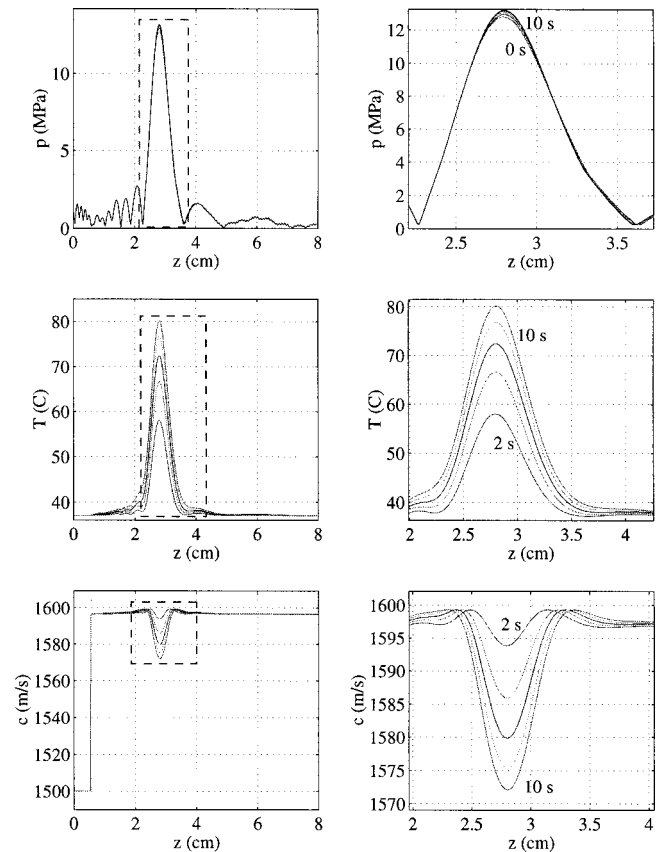


FIG. 4. The evolution of (a) p , (b) T , and (c) c_0 for the 1.0 MHz, F -no.=0.8 case with no fat layer, having 10 s duration. The curves on the right show enlarged version of the curves on the left in the vicinity of the focus (dotted outlines). Source power=66.1 W.

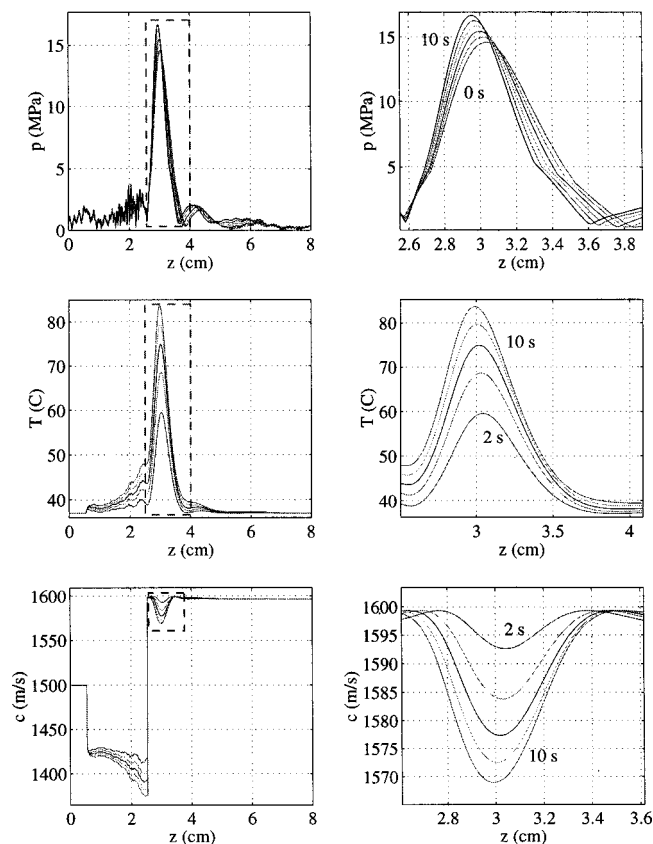


FIG. 5. The evolution of (a) p , (b) T , and (c) c_0 for the 1.0 MHz, F -no. = 0.8 case with a 2 cm fat layer, having 10 s duration. The curves on the right show enlarged version of the curves on the left in the vicinity of the focus (dotted outlines). Source power = 78.2 W.

layer changed readily with the relatively mild heating, according to the polynomial interpolation given in Eq. (6).

B. Short sonications at higher frequency (1.5 MHz)

Simulations using a 1.5 MHz source with similar geometry to the previously described F 1.0 source were carried out. This source resulted in very little thermo-acoustic lensing effect. We attribute this primarily to the higher focusing ability of high-frequency sources. In this case the fraction of energy heating the prefocal region and fat was smaller than for the 1.0 MHz runs of similar geometry due to the tighter focus. Even with a 2 cm fat layer in the prefocal region, this source resulted in a focal shift of about 0.5 mm only (Fig. 8).

C. Short sonications at lower gain (F no. = 1.3)

Simulations were also carried out using a 1.0 MHz source similar to those described previously, but having a longer radius of curvature (5.2 cm) for a F -number of 1.3. In these simulations both a 2 cm thick fat layer as well as a thicker 3.5 cm fat layer could be used. The results from these simulations are shown in Figs. 9 and 10. We see that for thicker fat layers more thermo-acoustic lensing occurs, especially when the focus is near the liver-fat interface. This is because when the focus is near the liver-fat interface, more acoustic energy is deposited in the fat, especially near the interface, and increased heating of the prefocal fat tissue occurs.

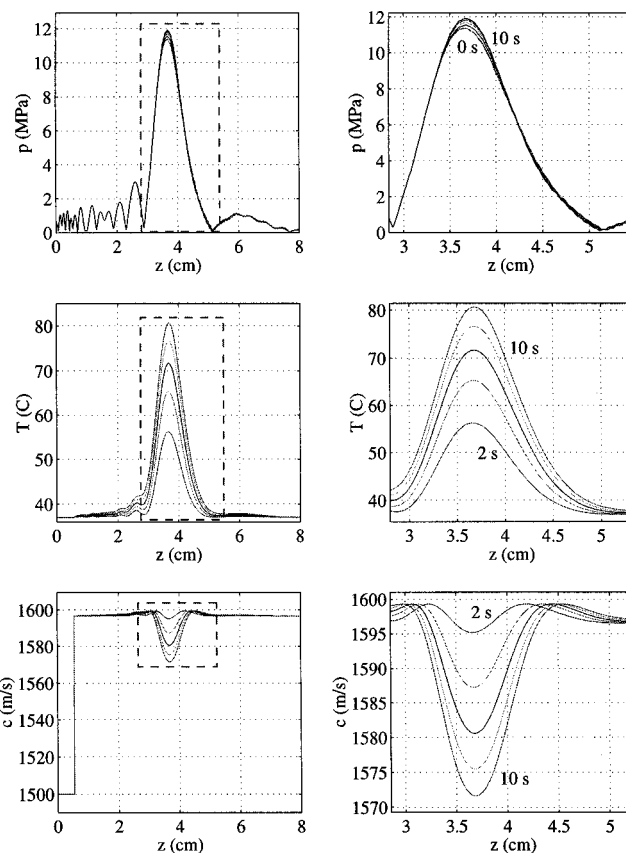


FIG. 6. The evolution of (a) p , (b) T , and (c) c_0 for the 1.0 MHz, F -no. = 1.0 case with no fat layer, having 10 s duration. The curves on the right show enlarged version of the curves on the left in the vicinity of the focus (dotted outlines). Source power = 82.1 W.

Some other data from the 3.5 cm fat layer simulation are shown for their illustrative value. Figure 11(a) presents a cross-axis view of the temperature near the focus at 10 s for runs with and without thermal lensing included. The thermal lens effect contributed an extra 10% to the peak temperature at the focus in this case. The hot spot's position and peak temperature were tracked and are presented in Fig. 11(b), which shows how the location of the maximum temperature moved toward the source in time. Finally, in Fig. 12, the 1 min and 240 min outlines of the calculated thermal dose at 43 °C are presented. The 1 min dose lines are presented to show the onset of multiple lesion development can occur at locations other than the intended focus in some cases, this being enhanced by the thermal lensing effect. The lesions formed with thermal lensing included were less elongated, more peaked, and were closer to the transducer than simulations without thermal lensing predicted.

D. Long (60 s) CW sonications

A set of simulations was carried out for the 1.0 MHz, F no. = 1.0 transducer, but at a lower power (60.5 W), such that without thermal lensing feedback the peak temperature after 60 s reached 80 °C. This resulted in more noticeable thermal lensing than the brief sonications described in the last sections. The comparison made was between a simulation in which the thermo-acoustic lens effect was modeled, and one in which the background sound speed of the tissue

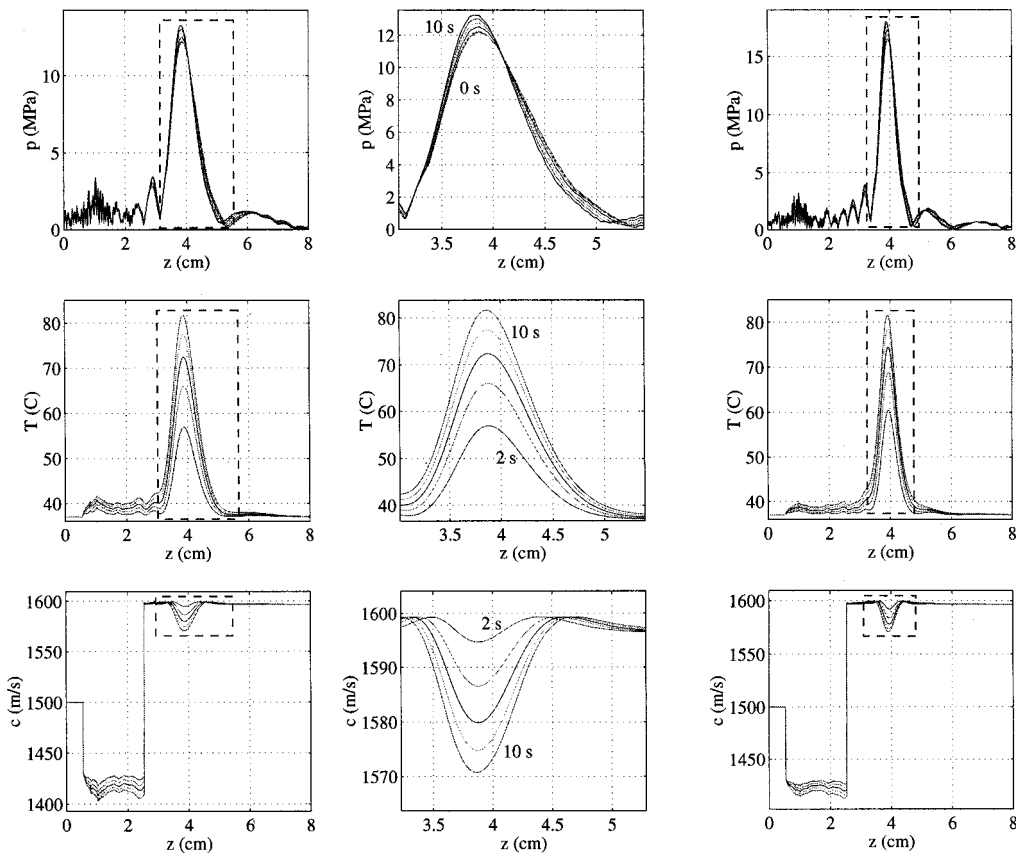


FIG. 7. The evolution of (a) p , (b) T , and (c) c_0 for the 1.0 MHz, F -no. = 1.0 case with a 2 cm fat layer, having 10 s duration. The curves on the right show enlarged version of the curves on the left in the vicinity of the focus (dotted outlines). Source power=98.1 W.

layers was held constant at its baseline value. Figure 13 shows the axial peak pressure, temperature, and sound speed. We see that the peak pressure is shifted by about 2 mm toward the source when acousto-thermal lensing occurs. The magnitude of the peak pressure also increases as the shape of the focal spot is changed. We also note an increase in peak temperature from a 60 s sonication in the presence of thermo-acoustic lensing. The location of the pressure and temperature maxima shifted about 2 mm overall.

Figure 14(a) shows the contours around the 240 min equivalent doses for the 60 s runs. Note that for this predictor of lesioning, very little movement or size change can be seen between simulations with and without the thermal lensing phenomenon. This is due to the similar temperature history for the sonications with and without thermal lensing included. The lesion predicted by the 240 min contours showed a slight (1 mm) movement toward the transducer and a slight change in shape. In Fig. 14(b) we compare the 240 min dose contours for the case without thermal lensing described above with a case where 60 s of cooling followed the 60 s of heating. The cooling stage made only a small contribution to the total volume of the predicted lesion. Finally, in Fig. 14(c) the temperature history of the geometric focus is shown for the case with no thermal lensing for a 60 s sonication followed by 60 s of cooling.

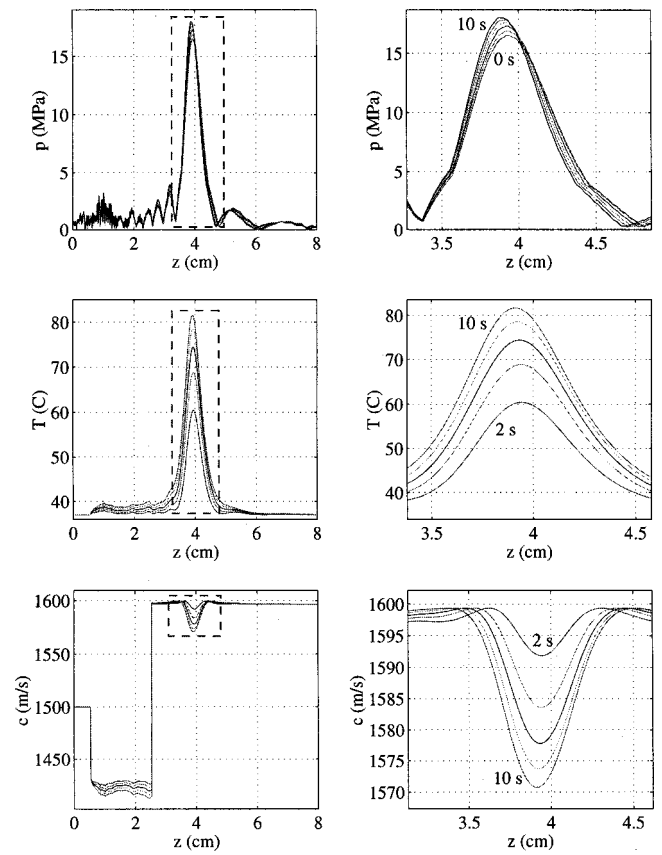


FIG. 8. The evolution of (a) p , (b) T , and (c) c_0 for the 1.5 MHz, F -no. = 1.0 case with a 2 cm fat layer, having 10 s duration. The curves on the right show enlarged version of the curves on the left in the vicinity of the focus (dotted outlines). Source power=65.2 W.

V. DISCUSSION

Simulations of acoustic pressure and temperature fields for focused ultrasound devices were performed showing the effect of varying sound speeds in tissues as a function of their temperature. Thermo-acoustic lensing effects were observed, and lead to a small migration of the focal hot spot during an FUS treatment. In addition, the peak temperatures were higher than those predicted by static models under similar conditions. The effects were due to the enhanced refraction of acoustic rays through the inhomogeneous media layers. The magnitude of the peak pressure and the peak temperature were also found to gradually increase for a steady CW source pressure as the thermo-acoustic lens developed. The maximum shift in the position of the focal spot for single brief (10 s) sonications was under 2 mm toward the source. The maximum difference in predicted peak temperature compared to the same simulations run without thermo-acoustic lensing was about 4 °C, or about a 10% difference in the temperature rise.

Specific effects noted were the effect of including a fat layer in front of the liver tissue, increasing the frequency by 50%, increasing the radius of curvature, and running a longer, lower power simulation. The main factors in producing thermo-acoustic lensing are the amount of prefocal heating which occurs along the propagation path, and the response of the medium along this path to heating. The higher F -number and the slow long sonications resulted in more

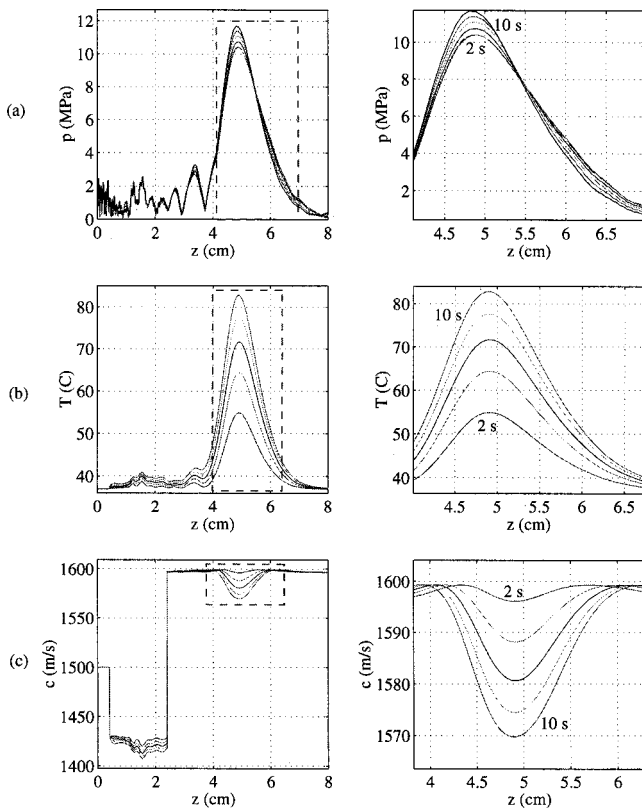


FIG. 9. The evolution of (a) p , (b) T , and (c) c_0 for the 1.0 MHz, F -no. = 1.3 case with a 2 cm fat layer, having 10 s duration. The curves on the right show enlarged version of the curves on the left in the vicinity of the focus (dotted outlines). Source power = 128.1 W.

pronounced thermal lensing. This effect was enhanced by the presence of the fat layer. In these simulations the fat acted to exaggerate the lensing because of the rapid descent in its sound speed as a function of temperature. Without the fat layer for short sonications almost no noticeable lensing was produced by the liver tissue alone (fractions of a mm). The increased frequency or decreased F -number resulted in reduced near-field heating and thermal lensing. We expect that sources with large focal spots that require longer sonications to achieve lesioning will result in more pronounced thermo-acoustic lensing. The same can be expected for phased array systems,^{33,7} which induce large lesions, for they will subject the prefocal tissue to more integrated thermal dose and heating over the duration of a FUS treatment.

Our model assumed that the dependence of sound speed on temperature was explicit, and used previously published data for the sound speed in fat and liver as a function of temperature to construct an interpolation polynomial which was periodically used to update the tissue sound-speed profiles. This model served as a starting point for investigating the phenomena of slowly varying tissue, and more work is needed to understand the mechanisms of change in tissue. Other time-varying material parameters can be modeled and inserted into the calculation loop. Data for variation of absorption coefficient are available for a limited set of conditions, but due to variations in measurement techniques, quantitative interpretation of this data remains unclear. Generally speaking, the absorption coefficient has been observed to increase with thermal dose and temperature.³⁴ A preliminary

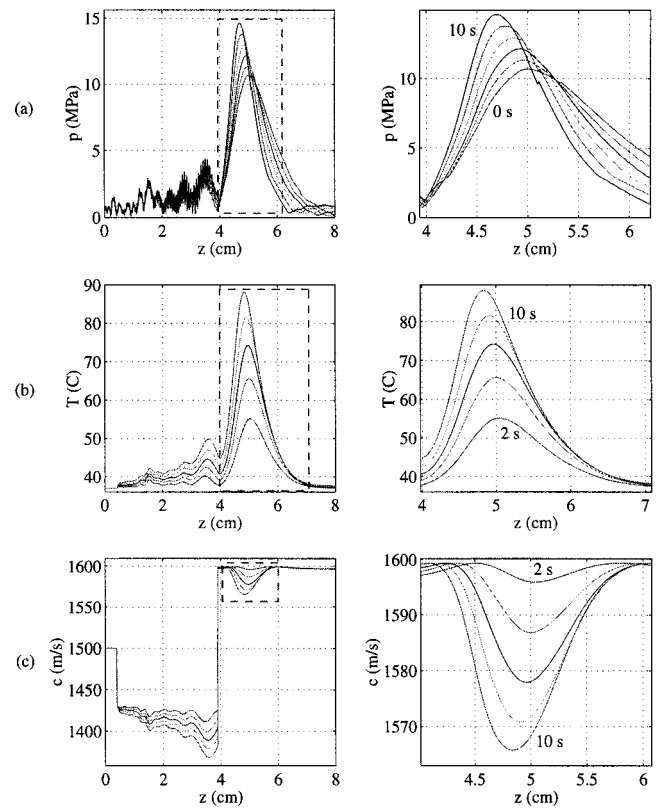


FIG. 10. The evolution of (a) p , (b) T , and (c) c_0 for the 1.0 MHz, F -no. = 1.3 case with a 3.5 cm fat layer, having 10 s duration. The curves on the right show enlarged version of the curves on the left in the vicinity of the focus (dotted outlines). Source power = 140.1 W.

study showed that the increase in local absorption near the focal region accelerated the heating rate and accompanying thermo-acoustic lens effect, and the increase was dependent on the temperature rise and the functional dependence of

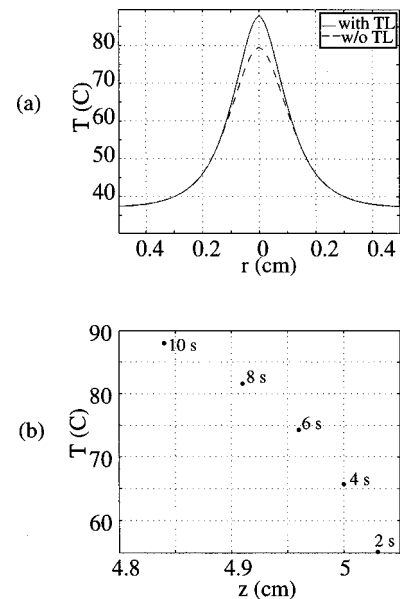


FIG. 11. (a) Slices of the peak temperature in the focal planes at 10 s for the $f = 1.0$ MHz F -no. = 1.3 case with 3.5 cm of fat with and without thermal lensing effect. (b) Movement of the peak temperature tracked at 2 s intervals for the $f = 1.0$ MHz F -no. = 1.3 case with 3.5 cm of fat and thermal lensing included.

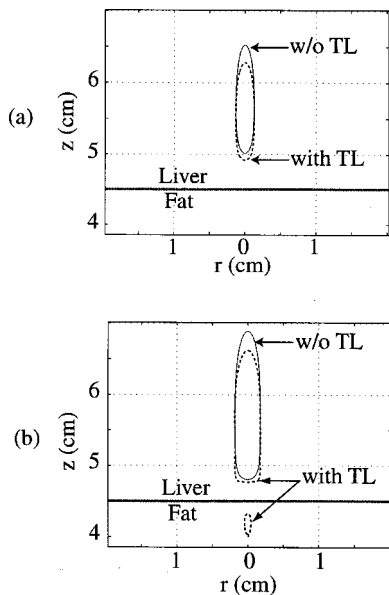


FIG. 12. Calculated thermal dose contours comparing the results from the $f=1.0$ MHz F -no.=1.3 with 3.5 cm of fat simulations with and without thermal lensing included. (a) The $t_{43}=240$ min dose outlines, (b) the $t_{43}=1$ min dose outlines.

absorption on temperature.²⁶ Equation (3) helps to explain how an acceleration of the thermo-acoustic interaction arises if α increases with temperature, because as the tissue is heated α would increase, leading to a higher heating rate,

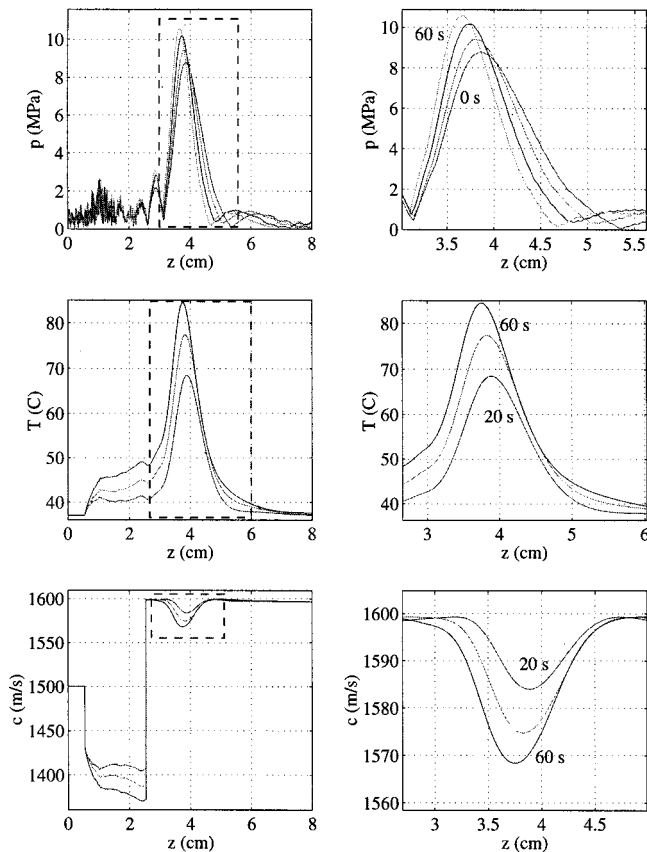


FIG. 13. The evolution of (a) p , (b) T , and (c) c_0 for the 1.0 MHz, F -no.=1.0 case with a 2 cm fat layer, having 60 s duration. The curves on the right show enlarged version of the curves on the left in the vicinity of the focus (dotted outlines). Source power=60.5 W.

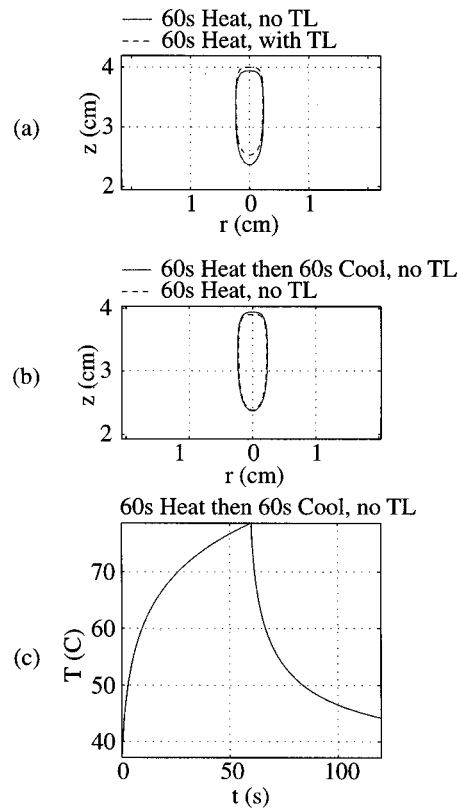


FIG. 14. The outlines of the calculated $t_{43}=240$ min dose curves (a) with and without thermal lensing, (b) with and without subsequent cooling, (c) the temperature at the focus, for the long sonication case with $f=1$ MHz, F -no.=1.0 at 60.5 W.

and faster rising temperatures. However, because the effect would be most significant in a local area near the focus only, it is not expected that this effect would significantly contribute to thermal lensing. Data for other properties, such as the temperature-dependence of the nonlinearity coefficient and the density, are not readily available for most tissues.

In conclusion, the dependence of sound speed on tissue temperature appears to have a minor impact on the coagulated tissue volume or its location for brief sonications from single-focus sources having F -numbers around 1.0 and frequencies around 1.0 MHz, as commonly used in clinical ultrasound surgery systems. This result may not apply to multiple-focus arrays or scanned systems, which produce much higher near-field thermal doses. In such systems, the prefocal regions experience the effects of repeated overlapping sonications or scans, while the smaller focal zones are only heated by their respective individual sonications. Since the thermal lens effect is a cumulative path effect of propagation from the source to the focus, it is most significant for propagation through a long path of heated tissue, such as the prefocal tissue in scanned or multifocal array systems.

ACKNOWLEDGMENT

This work was supported in part by the National Cancer Institute (Grant No. R01:CA46627).

- ¹F. J. Fry, "Intense focused ultrasound in medicine," *Eur. Urol.* **23**(Suppl I), 2–7 (1993).
- ²N. Sanghvi and R. Hawes, "High intensity focused ultrasound," *Exper. & Investigational Endoscopy* **4**, 383–395 (1994).
- ³C. Hill and G. ter Haar, "Review article: High intensity focused ultrasound—potential for cancer treatment," *Br. J. Radiol.* **68**, 1296–1303 (1995).
- ⁴K. Hynynen, R. Roemer, E. Moros, C. Johnson, and D. Anhalt, "The effect of scanning speed on temperature and equivalent thermal exposure distributions during ultrasound hyperthermia *in vivo*," *IEEE Trans. Microwave Theory Tech.* **34**, 552–559 (1986).
- ⁵G. ter Haar, "Ultrasound focal beam surgery," *Ultrasound Med. Biol.* **3**, 1089–1100 (1995).
- ⁶C. Damianou, K. Hynynen, and X. Fan, "Evaluation of accuracy of a theoretical model for predicting the necrosed tissue volume during focused ultrasound surgery," *IEEE Trans. Ultrason. Ferroelectr. Freq. Control* **42**, 182–187 (1995).
- ⁷D. Daum, N. Smith, R. King, and K. Hynynen, "*In vivo* demonstration of noninvasive thermal surgery of the liver and kidney using an ultrasonic phased array," *Ultrasound Med. Biol.* **25**, 1087–1098 (1999).
- ⁸J. Wu and G. Du, "Temperature elevation in tissues generated by finite-amplitude tone bursts of ultrasound," *J. Acoust. Soc. Am.* **88**, 562–577 (1990).
- ⁹C. Hill, I. Rivens, M. Vaughan, and G. ter Haar, "Lesion development in focused ultrasound surgery: A general model," *Ultrasound Med. Biol.* **20**, 259–260 (1994).
- ¹⁰X. Fan and K. Hynynen, "Ultrasound surgery using multiple sonications—Treatment time considerations," *Ultrasound Med. Biol.* **22**, 471–481 (1996).
- ¹¹X. Fan and K. Hynynen, "The effect of wave reflection and refraction at soft tissue interfaces during ultrasound hyperthermia treatments," *J. Acoust. Soc. Am.* **91**, 1727–1736 (1992).
- ¹²H. Wan, P. VanBaren, E. Ebbini, and C. Cain, "Ultrasound surgery: comparison of strategies using phased array systems," *IEEE Trans. Ultrason. Ferroelectr. Freq. Control* **43**, 1085–1098 (1996).
- ¹³H. Pennes, "Analysis of tissue and arterial blood temperature in the resting human forearm," *J. Appl. Phys.* **1**, 93–122 (1948).
- ¹⁴P. Lele and A. Pierce, "The thermal hypothesis of the mechanism of ultrasonic focal destruction in organized tissues," *Proceedings of the workshop on Interaction of Ultrasound and Biological Tissues*, Bureau of Radiological Health, FDA 73-8008, pp. 121–128 (1973).
- ¹⁵W. Nyborg, "Heat generation by ultrasound in a relaxing medium," *J. Acoust. Soc. Am.* **70**, 310–312 (1981).
- ¹⁶M. Curley, "Soft tissue temperature rise caused by scanned, diagnostic ultrasound," *IEEE Trans. Ultrason. Ferroelectr. Freq. Control* **40**, 59–66 (1993).
- ¹⁷J. Wu, J. Chase, and T. Holzapfel, "Temperature rise in a tissue-mimicking material generated by unfocused and focused ultrasonic transducers," *Ultrasound Med. Biol.* **5**, 495–512 (1992).
- ¹⁸K. Hynynen, "Demonstration of enhanced temperature elevation due to nonlinear propagation of focussed ultrasound in dog's thigh *in vivo*," *Ultrasound Med. Biol.* **13**, 85–91 (1987).
- ¹⁹M. Kolios, A. Worthington, M. Sherar, and J. Hunt, "Experimental evaluation of two simple thermal models using transient temperature analysis," *Phys. Med. Biol.* **43**, 3325–3340 (1992).
- ²⁰L. Chen, G. ter Haar, D. Robertson, J. Bensted, and C. Hill, "Histological study of normal and tumor-bearing liver treated with focused ultrasound," *Ultrasound Med. Biol.* **25**, 847–856 (1999).
- ²¹C. Le Floch, M. Tanter, and M. Fink, "Self-defocusing in ultrasonic hyperthermia: Experiment and simulation," *Appl. Phys. Lett.* **74**, 3062–3064 (1999).
- ²²R. Seip, P. VanBaren, C. Cain, and E. Ebbini, "Noninvasive real-time multipoint temperature control for ultrasound phased array treatments," *IEEE Trans. Ultrason. Ferroelectr. Freq. Control* **43**, 1063–1073 (1996).
- ²³J. Lu, H. Ying, Z. Sun, M. Motamedi, B. Bell, and L. Sheppard, "*In vitro* measurement of speed of sound during coagulate tissue heating," in *Proceedings of the IEEE Ultrasonics Symposium*, pp. 1299–1302 (1996).
- ²⁴M. F. Hamilton and C. L. Morfey, "Model equations," in *Nonlinear Acoustics*, edited by M. F. Hamilton and D. T. Blackstock (Academic, San Diego, 1998), Chap. 3.
- ²⁵R. T. Beyer, "The Parameter B/A " in *Nonlinear Acoustics*, edited by M. F. Hamilton and D. T. Blackstock (Academic, San Diego, 1998), Chap. 2.
- ²⁶I. Hallaj, R. Cleveland, R. Roy, and R. Holt, "Coupled thermal-acoustic simulation results with temperature-dependent tissue parameters for therapeutic ultrasound," *J. Acoust. Soc. Am.* **104**, 1844(A) (1998).
- ²⁷I. Hallaj and R. Cleveland, "FDTD simulation of finite-amplitude pressure and temperature fields from biological ultrasound," *ARLO* **1**, 7–12 (1999).
- ²⁸S. Goss, R. Johnston, and F. Dunn, "Comprehensive compilation of empirical ultrasonic properties of mammalian tissues," *J. Acoust. Soc. Am.* **64**, 423–457 (1978).
- ²⁹A. D. Pierce, *Acoustics, An Introduction to its Physical Principles and Applications* (AIP Press, Woodbury, NY, 1989), Chap. 10.
- ³⁰S. Sapareto and W. Dewey, "Thermal dose determination in cancer therapy," *Int. J. Radiat. Oncol., Biol., Phys.* **10**, 787–800 (1984).
- ³¹J. Bamber and C. Hill, "Ultrasonic attenuation and propagation speed in mammalian tissues as a function of temperature," *Ultrasound Med. Biol.* **5**, 149–157 (1979).
- ³²R. Schechter, K. Simmonds, R. Mignogna, and P. Delsanto, "Use of a transient wave propagation code for 3D simulation of CW radiated transducer fields," *Ultrasonics* **37**, 89–96 (1999).
- ³³S. Umemura and C. Cain, "The sector-vortex phased array: Acoustic field synthesis for hyperthermia," *IEEE Trans. Ultrason. Ferroelectr. Freq. Control* **36**, 249–257 (1989).
- ³⁴C. Damianou, N. Sanghvi, F. Fry, and R. Maas-Moreno, "Dependence of ultrasonic attenuation and absorption in dog soft tissues on temperature and thermal dose," *J. Acoust. Soc. Am.* **102**, 628–634 (1997).
- ³⁵E. Carstensen, S. Becroft, W. Law, and D. Barbee, "Finite amplitude effects on the threshold for lesion production in tissues by unfocused ultrasound," *J. Acoust. Soc. Am.* **70**, 302–309 (1981).